Extreme upper level cyclonic vorticity events in relation to the Southern Hemisphere jet stream

N. Harnik

Department of Geophysics and Planetary Sciences, Tel Aviv University, Tel Aviv, 69978, Israel

---

N. Harnik, Department of Geophysics and Planetary Sciences, Tel Aviv University, Israel. (harnik@tau.ac.il)

The climatological seasonal variation in the frequency of occurrence of extreme upper level cyclonic vorticity events, and its relation to the jet stream, is examined in the Southern Hemisphere. During summer-fall, extreme cyclonic vorticity occurs most frequently at the upper level jet stream core, while during winter-spring, there is a main peak on the poleward flank of the subtropical jet, and a secondary peak on the poleward flank of the eddy driven jet. Composite analysis shows that the extremes in both seasons are associated with wave breaking and the formation of elongated vorticity tongues. In summer, extreme vorticity values occur when waves propagating on the eddy driven jet break nonlinearly while in winter, extreme values occur when waves on the eddy driven jet interact with waves on the subtropical jet. In both seasons, these upper level extreme values are associated with significant surface temperature and precipitation anomalies.

1. Introduction

The anomalous Hemispheric-wide winter conditions of the recent Northern Hemisphere winter (2013-14) have raised interest in what controls the distribution and frequency of extreme events, and how those might change with the large scale atmospheric circulation. As pointed out by the recent Science letter by *Wallace et al.* [2014], a preliminary examination of this past winter's flow suggests the extreme weather conditions arose, at least partly, from large undulations in the mid-latitude jet stream and the stratospheric polar vortex, with no clear proven relation to global warming or arctic sea-ice melting. In fact, for most types of extreme events, we do not understand their relation to the large scale atmospheric circulation well enough to be able to predict how they might change with climate.

Intuitively, we expect the distribution of extreme events to be linked to the large scale flow. However there are many types of extremes, each with their corresponding impacts, each involving different processes ranging from micro scale to global scale, making the relation to the highly complex atmosphere-climate system quite elusive. At the simplest level, extreme values of a given field are related to basic statistical quantities of its distribution, like the mean, standard deviation, and skew. For quantities like wind speed and vorticity, which describe the atmospheric flow field, the basic statistical quantities are directly linked to the structure of the jet streams and synoptic storms. Fields like temperature and precipitation which are more directly affected by physical processes like radiation, micro scale processes in clouds, and the interaction with the land, ice or sea surface below, are also affected by the jet stream and its large scale undulations, partly indirectly through the jet stream's influence on the location and evolution of synoptic storms. Indeed, various studies have examined the relation of extremes to large scale patterns of variability (partial list: surface extremes in relation to North Atlantic jet latitude [*Mahlstein et al.*, 2012], to common modes of variability in the Northern Hemisphere [*Donat et al.*, 2010; *Kenyon and Hegerl*, 2008, 2010; *Scaife et al.*, 2008; *Franzke*, 2013], Southern Hemisphere [*England et al.*, 2006; *Ummenhofer and England*, 2007], and to large scale flow features [*Raible*, 2007, e.g]).

We will take a different focus, and examine the influence of one of the central characteristics of the global circulation- the jet stream type - on extreme events. Meteorologists have long noticed two types of jet streams- subtropical jets which form due to meridional advection of angular momentum by the Hadley circulation [e.g. *Schneider*, 1977; *Held and Hou*, 1980], and polar front jets, also referred to as eddy-driven jets, which form due to the convergence of momentum by the synoptic storms [e.g. *Panetta*, 1993]. The interaction of these two types of jets with synoptic storms is correspondingly very different, resulting in very different latitudinal locations, vertical structures and temporal variations [*Lee and Kim*, 2003; *Eichelberger and Hartmann*, 2007]. Thus, while the thermally driven subtropical jet is strongly baroclinic and its latitudinal position is relatively constant with time, the eddy driven jet has a strong surface westerly component, and it meanders strongly in its latitudinal position.

The Southern Hemisphere jet stream undergoes a sharp seasonal transition, from a dominantly thermally driven subtropical jet during winter, to an eddy driven mid latitude jet during summer [e.g *Nakamura et al.*, 2004]. In this study we will make use of this transition, and examine how the distribution of extreme upper level vorticity events changes seasonally. This will provide at least an upper bound on the degree to which the large scale flow, in particular the location and strength of the jet stream, affect extremes. We choose to examine extreme values of upper level cyclonic vorticity because we expect it to be more strongly affected by the large scale circulation compared to the more traditional fields used for studying extreme weather events (e.g. surface temperature or precipitation), but at the same time we expect it to be indicative of extreme weather. We expect extreme vorticity values to be associated with a deep upper level trough, and with wave breaking and the formation of potential vorticity (PV) streamers, both of which have been shown to play a role in the formation of extreme weather conditions (e.g. extreme precipitation [*Martius et al.*, 1006, 2013; *Romero et al.*, 1999; *Jacobeit*, 1987; *Krichak et al.*, 2007; *Massacand et al.*, 1998], Brazilian cold surges [*Sprenger et al.*, 2012]). We start by examining how the climatological frequency of occurrence of extreme negative vorticity values varies spatially and seasonally, in relation to the type of jet stream. We will then show that indeed the formation of these extreme values is associated with wave breaking and examine the differences in its evolution between the two solstice seasons, again in relation to the jet stream structure and location.

2. Data and diagnostics

We use daily mean wind fields from ERA Interim [*Dee et al.*, 2011] for years 1979-2012 and NCEP re-analysis [*Kalnay et al.*, 1996] for years 1959-2012. Vorticity ζ is calculated from the daily horizontal winds (u in the longitudinal direction λ and v in the latitudinal direction φ):

$$\zeta = \frac{1}{a_e \cos\varphi}\frac{\partial v}{\partial \lambda} - \frac{1}{a_e \cos\varphi}\frac{\partial (u\cos\varphi)}{\partial \varphi} \quad (1)$$

where a_e is the Earth's radius. We define an extreme cyclonic vorticity event when ζ drops below the lowest 1% of vorticity values of all days and all grid points within the Southern Hemisphere. We then calculate the frequency of occurrence of extreme events as a function of spatial location or day of the year. Since the two reanalysis data sets differ in spatial resolution and in temporal extent, we have 1.72 times more data points for ERA Interim compared to NCEP. As a result, the probability distribution function of all occurring vorticity values is shifted to lower values for NCEp. We thus restrict the comparison to the seasonal and latitudinal shape of the distribution, and not to the absolute values.

We use composite analysis to obtain a characteristic evolution of the extreme events in different seasons, at the latitude of most frequent occurrence. For extreme vorticity events for which the threshold is exceeded for more than one day in a row, we only choose the day with most extreme value. We also isolate the events spatially, discounting extreme values within 30 degrees longitude on each side of the event peak and then centre them around the peak longitude. The composites are only done for the very most extreme events, with the threshold chosen to give around 250 events, but the results are not sensitive to the exact value of this threshold. Statistical significance is calculated using a bootstrap method, with the null hypothesis being a characteristic wave packet, given that wave packets are prominent upper level flow features. To do this, we create a daily wave packet data base, by finding the longitude at which the vorticity anomaly peaks at the latitude of the composite centre, and centering the vorticity field around this longitude. We then randomly choose 1000 combinations of NComp days, where NComp is the number of events in our composite, and get a distribution of randomly chosen wave packet composites. Those grid points in the composite for which the anomaly is outside the 1000-member random distribution are considered statistically significant (e.g. 99.9% significance). The composites are done both for full fields and for the anomalies, defined as the deviation from the climatological seasonal cycle. The statistical significance, however, is determined purely from the anomaly fields. The climatological seasonal cycle is calculated by averaging the given field for each calendar day over all years, and applying a 21 day running mean for smoothing.

3. Results

Figure 1 shows the seasonal-latitudinal distribution of the frequency of occurrence of extreme negative (cyclonic) vorticity events, for ERA Interim and NCEP reanalyses, while Fig. 2 shows the spatial distribution of extreme events during the two solstice seasons (Jan-Mar and Jun-Aug), using the higher resolution ERA Interim data. The climatological seasonal cycle (Fig. 1) was created by counting the number of extreme events which occurred at each latitude and each calendar date (excluding Feb 29^{th}) while the spatial distribution maps (Fig. 2) were calculated by counting the number of days with extreme values at each grid point. The seasonal maps were divided by the number of years times the number of longitude grid points, and the spatial maps by the total number of days, to get a probability of occurrence. Also shown on both plots are the climatological zonal mean winds at 300 hPa and at $925-750$ hPa, representing the upper level jet stream, and the lower level eddy driven jet respectively. The figures reveal a strong relation between the distribution of extreme events and the jet stream. We see a clear seasonal cycle which roughly follows the upper level jet stream, captured quite similarly by the two reanalyses (Fig. 1). During summer and fall (Dec-Apr, Fig. 1, Fig. 2top), the upper and lower level jets coincide, indicative of a strong barotropic eddy-driven jet [*Son and Lee*, 2005, e.g.]. The jets are also quite zonally symmetric, and the extreme cyclonic vorticity events occur most frequently at this jet core. We note that the the vorticity of the mean flow peaks at the jet flanks, suggesting the eddy fields are dominant in their contribution to extreme cyclonic vorticity values.

The picture is very different during winter and early spring (Jun-Oct, Fig.1, Fig.2 bottom) when it assumes a spiral structure. Over the Indian and Pacific oceans it has characteristics of a thermally-driven subtropical jet, while elsewhere, it has characteristics of a mid-latitude eddy driven jet [*Nakamura and Shimpo*, 2004]. In the zonal mean, we see an upper level subtropical jet (at the edge of the Hadley cell, not shown), alongside a mid-latitude lower level eddy-driven jet. In clear relation to the jet structure, the distribution of extreme cyclonic vorticity values splits with a main peak on the poleward flank of the upper level subtropical jet (confined like the jet to the Indian and Pacific Oceans), and a secondary peak on the poleward flank of the lower level eddy driven jet. Unlike in summer, the negative vorticity of the mean flow contributes partly to the extreme negative vorticity values. In particular, extreme vorticity anomalies (deviations from a seasonal cycle) have a single peak at the core of the subtropical jet, with no significant peak in higher latitudes (not shown).

To further examine the differences between the extreme events during these two time periods, we composite various fields around the extreme events at the peak latitude of the distribution, for the different winter and summer jet types. Fig 3 shows the composites of 300 hPa geopotential height anomalies for the extreme Jan-Mar cyclonic vorticity events at 49.5^oS and for the Jun-Aug events at 33^oS, between $50^oE - 250^oE$, each overlain on the centered and time averaged (time lags $-6 : 6$ days) composite of upper level zonal winds. Fig 4 shows composites of 300 hPa absolute vorticity, a quantity which nicely tracks the overturning of vorticity contours during Rossby wave breaking events [*Barnes and Hartmann*, 2012], along with a composite of precipitation and surface temperature anomaly.

Looking at the geopotential height and absolute vorticity composites, we see different flow evolutions between the two seasons. During Jan-Mar we see an upper level wave packet propagating on the jet stream (days -5, -3), growing in amplitude until it breaks and forms an elongated tongue of low vorticity which deepens at the event centre ($day0$). We note that the wave breaking starts when the wave packet moves into a region where the zonal jet stream is weakest (between days -3 and 0), consistent with *Swanson et al.* [1997], while the wave breaking further weakens the jet at this location (seen from examining the zonal wind composites for individual days, not shown). The deepening of the low absolute vorticity centre, seen also in geopotential height, indicates contribution from stretching (supported by composites of potential temperature, not shown). This suggests the absolute vorticity tongue is part of a PV streamer which forms during these events.

During Jun-Aug the extreme cyclonic vorticity also develops when an existing wave packet strengthens and breaks to form a vorticity tongue, but in contrast to the summer case, the extreme negative vorticity anomaly on the thermally driven subtropical jet involves interaction with waves on the midlatitude eddy driven jet. This is seen clearly in the geopotential height field. On day -5 we see a midlatitude wavepacket on the midlatitude jet at upstream longitudes of $-280^o - -110^o$ which splits into one wavepacket on the subtropical jet (upstream longitudes of $-140^o - -80^o$) and another wavepacket propagating polewards along the higher latitude eddy driven jet. On day -3, the anomalies from the two jets merge, coincident with the formation of a southward-elongated high-vorticity tongue, with wave breaking evolving to produce the extremely negative vorticity values by day 0. A very similar upper level geopotential height evolution was observed by *Marengo et al.* [2002], in relation to extreme winter cold surges in Brazil, suggesting the upper level vorticity anomalies are relevant also to surface weather.

A surface influence is indeed found for both seasons, as can be seen from the day 0 composites of surface temperature and precipitation (Fig. 4, right plots). We see for both seasons, significant localized cold ($1.5 - 2^oC$) and warm (around 1^oC) temperature anomalies associated with northward and southward temperature advection to the northwest and east of the extreme cyclonic vorticity centre, and a significant precipitation anomaly of about $1.2mm/day$ to the north-east of the vorticity center. These surface anomalies are consistent with the dynamical evolution around PV streamers [as summarized in *Schlemmer et al.*, 2010]. We also see, a weaker but significant warm temperature anomaly (0.5^oC) in mid latitudes, west of the event centre. During Jan-Mar the surface temperature anomalies are zonally aligned between $55^oS - 30^oS$, while during Jun-Aug the anomalies span a larger latitude range, with a very large (in area) cold anomaly on the poleward flanks of the midlatitude eddy driven jet, alongside a significant low geopotential height anomaly (Fig 3 lower right). This is consistent with the Jan-Mar event involving waves on the eddy driven jet, and the Jun-Aug event involving waves on the midlatitude eddy driven and subtropical thermally driven jets.

4. Conclusion

The spatial distribution of extreme upper level negative vorticity events varies seasonally in a manner which is clearly related to the seasonal evolution of the zonal jet stream. The spatial relation to the jet position also varies seasonally. During summer, when the jet is eddy driven and in midlatitudes, the extreme events occur most frequently at the jet center. During winter, on the other hand, the upper level jet is in the subtropics, and strongly thermally driven, while the lower level jet is in midlatitudes, and the extreme events occur most frequently on the poleward flank of the upper level subtropical jet, with a secondary peak on the poleward flank of the midlatitude eddy driven jet. This difference in position relative to the jet comes along with differences in the characteristic temporal evolution of the extreme vorticity events (as seen from a composite analysis). While during summer, waves propagating on the jet break and form a negative vorticity anomaly at the jet core, during winter, the wave breaking involves an interaction between anomalies on the subtropical and midlatitude jets, so that the extreme vorticity values form on the poleward flank of the subtropical jet.

The differences in temporal evolution make sense given the different dynamical balances which lead to the different jet types. The subtropical latitude of the thermally driven jet reduces its baroclinic instability [due to large β, *Lachmy and Harnik*, 2014]. Moreover, it peaks at the edge of the Hadley cell, where the eddy momentum flux convergence is zero [*Son and Lee*, 2005, e.g]. Thus, this type of jet can only be sustained in the presence of weak enough eddies [*Lachmy and Harnik*, 2014]. Correspondingly, cyclogenesis and baroclinic growth (e.g. as indicated by transient eddy heat fluxes) are strongest in mid and high latitudes, and in particular, during winter, they are weakest at the longitudes where the subtropical jet is strongest [e.g *Simmonds and Keay*, 2000; *Nakamura et al.*, 2004; *Lachmy and Harnik*, 2014]. The peak in the occurrence of extreme vorticity values at the subtropical jet during winter, despite the weaker wave growth, seems to be enabled only through an interaction with the mid-latitude jet waves. We are currently examining this hypothesis in idealized models.

The relevance of extreme upper level vorticity to extreme surface weather needs to be further examined. Our composite analysis (Fig. 4, right plots) suggests extreme upper level cyclonic vorticity values are associated with significant surface temperature and precipitation anomalies. While the composited temperature anomalies are not very large, unrelated studies of extreme cold anomalies point to a link to upper level flow. In particular, *Sprenger et al.* [2012] and *Marengo et al.* [2002] found cold surges in Brazil to be associated with wave breaking and PV streamer formation, and with upper level geopotential height patterns very similar to Fig. 3, while *Ashcroft et al.* [2009] found extreme

Australian cold events to be associated with a temporary merging of the subtropical and mid latitude jet streams.

To summarize, we find that the distribution of extreme upper level vorticity undergoes significant seasonal changes, which clearly follow the jet stream. Preliminary analyses of the extremes of other variables also suggests strong dynamical relations. By nature of the problem, detecting and predicting future changes in the distribution of extreme events involves a high degree of uncertainty, and requires much larger observational records than other dynamical studies. In the future, a better understanding of the dynamical relations to the large scale flow can hopefully be incorporated to improve statistical studies and prediction of extreme events.

Acknowledgments. The work was supported by the Israeli Science Foundation grant number 1537/12. All calculations presented here were performed using GOAT (Geophysical Observation Analysis Tool), a freely available MATLAB based tool for retrieval, analysis and visualization of geophysical data (http://www.goat-geo.org). The author thanks Ori Adam for help with GOAT, Chaim Garfinkel for helpful discussions and comments on the manuscript, and Orli Lachmy for helpful tips on the composite calculations. ECMWF ERA-Interim data used in this study have been obtained from the ECMWF Data Server http://data-portal.ecmwf.int/data/d/interim_daily/ . NCEP Reanalysis data was provided by the NOAA/OAR/ESRL PSD, Boulder, Colorado, USA, from their Web site at http://www.esrl.noaa.gov/psd/.

References

Ashcroft, L. C., A. B. Pezza, and I. Simmonds (2009), Cold events over southern australia: Synoptic climatology and hemispheric structure, *JClim*, *22*, 6679–6698.

Barnes, E. A., and D. L. Hartmann (2012), Detection of rossby wave breaking and its response to shifts of the midlatitude jet with climate change, *J. Geophys. Res.*, doi: 10.1029/2012JD017469.

Dee, D. P., et al. (2011), The ERA-Interim reanalysis: configuration and performance of the data assimilation system., *Q. J. R. Meteorol. Soc.*, *137*, 553–597.

Donat, M. G., G. C. Leckebusch, J. G. Pinto, and U. Ulbrich (2010), Examination of wind storms over central europe with respect to circulation weather types and nao phases, *Int. J. Climatol.*, *30*.

Eichelberger, S. J., and D. L. Hartmann (2007), Zonal jet structure and the leading mode of variability, *J. Clim.*, p. 51495163.

England, M. H., C. C. Ummenhofer, and A. Santoso (2006), Interannual rainfall extremes over southwest western australia linked to indian ocean climate variability, *J. Clim.*, *19*, 1948–1969.

Franzke, C. (2013), Persistent regimes and extreme events of the north atlantic atmospheric circulation, *Phil. Trans. R. Soc. A*, *371*, 20110,471.

Held, I. M., and A. Y. Hou (1980), Nonlinear axially-symmetric circulations in a nearly inviscid atmosphere, *J. Atmos. Sci.*, *37*, 515–533.

Jacobeit, J. (1987), Variations of trough positions and precipitation patterns in the mediterranean area, *J. Climatol.*, *7*, 453–476.

Kalnay, E., et al. (1996), The NCEP/NCAR 40-year reanalysis project, *B. Am. Meteorol. Soc.*, *77*(434-471).

Kenyon, J., and G. C. Hegerl (2008), Influence of modes of climate variability on global temperature extremes, *J. Clim.*, *21*, 3872–3889.

Kenyon, J., and G. C. Hegerl (2010), Influence of modes of climate variability on global precipitation extremes, *J. Clim.*, *23*, 6248–6262.

Krichak, S. O., P. Alpert, and M. Dayan (2007), A southeastern mediterranean pv streamer and its role in december 2001 case with torrential rains in israel, *Nat. Hazards Earth Syst. Sci.*, *7*, 21–32.

Lachmy, O., and N. Harnik (2014), The transition to a subtropical jet regime and its maintenance, *J. Atmos. Sci.*, *71*, 1389–1409.

Lee, S., and H. K. Kim (2003), The dynamical relationship between subtropical and eddy-driven jets, *J. Atmos. Sci.*, *60*, 1490–1503.

Mahlstein, I., O. Martius, C. Chevalier, and D. Ginsbourger (2012), Changes in the odds of extreme events in the atlantic basin depending on the position of the extratropical jet, *Geophys. Res. Lett.*, *39*, L22805.

Marengo, J. A., T. Ambrizzi, G. Kiladis, and B. Liebmann (2002), Upper-air wave trains over the pacific ocean and wintertime cold surges in tropical-subtropical south america leading to freezes in southern and southeastern brazil, *Theor. Appl. Clim.*, *73*, 223–242.

Martius, O., E. Zenklusen, C. Schwierz, and H. C. Davies (1006), Episodes of alpine heavy precipitation with an overlying elongated stratospheric intrusion: A climatology, *Int. J. Climatol.*, *26*, 1149–1164.

Martius, O., H. Sodemann, H. Joos, S. Pfahl, A. Winschall, M. Croci-Maspoli, M. Graf, E. Madonna, B. Mueller, S. Schemm, J. Sedlek, M. Sprenger, and H. Wernli (2013), Upper-level dynamics and surface processes for the pakistan flood in july 2010, *Q. J. R. Meteorol. Soc.*, *139*, 1780–1797.

Massacand, A. C., H. Wernli, and H. C. Davies (1998), Heavy precipitation on the alpine southside: An upper-level precursor, *Geophys. Res. Lett.*, *25*, 14351438.

Nakamura, H., and A. Shimpo (2004), Seasonal variations in the southern hemisphere storm tracks and jet streams as revealed in a reanalysis dataset., *J. Clim.*, *17*, 1828–1844.

Nakamura, H., T. Sampe, Y. Tanimoto, and A. Shimpo (2004), Observed associations among storm tracks, jet streams and midlatitude oceanic fronts, *Geophysical Monograph Series*, *147*, 329–345.

Panetta, R. L. (1993), Zonal jets in wide baroclinically unstable regions: Persistence and scale selection, *J. Atmos. Sci.*, *50*, 2073–2106.

Raible, C. C. (2007), On the relation between extremes of midlatitude cyclones and the atmospheric circulation using ERA40, *Geophys. Res. Lett.*, *34*, doi: 10.1029/2006GL029084.

Romero, R., G. Sumner, C. Ramis, and A. Genoves (1999), A classification of the atmospheric circulation patterns producing signficant daily rainfall in the spanish mediterranean area., *Int. J. Climatol.*, *19*, 765–785.

Scaife, A., C. Folland, L. Alexander, A. Moberg, and J. Knight (2008), European climate extremes and the north atlantic oscillation, *J. Clim.*, *21*, 72–83.

Schlemmer, L., O. Martius, M. Sprenger, C. Schwierz, and A. Twitchett (2010), Disentangling the forcing mechanisms of a heavy precipitation event along the alpine south side using potential vorticity inversion., *Mon. Wea. Rev.*, *138*, 2336–2353, doi: 10.1175/2009MWR3202.1.

Schneider, E. K. (1977), Axially symmetric steady-state models of the basic state for instability and climate studies. part II. nonlinear circulations, *J. Atmos. Sci.*, *34*, 280–296.

Simmonds, I., and K. Keay (2000), Mean southern hemisphere extratropical cyclone behavior in the 40-year ncepncar reanalysis, *J. Clim.*, *13*, 873–885.

Son, S. W., and S. Lee (2005), The response of westerly jets to thermal driving in a primitive equation model, *J. Atmos. Sci.*, *62*, 3741–3757.

Sprenger, M., O. Martius, and J. Arnold (2012), Cold surge episodes over southeastern brazil - a potential vorticity perspective, *Int. J. Climatol.*, *33*, 2758–2767.

Swanson, K. L., P. J. Kushner, and I. M. Held (1997), Dynamics of barotropic storm tracks, *J. Atmos. Sci.*, *54*, 791–810.

Ummenhofer, C. C., and M. H. England (2007), Interannual extremes in new zealand precipitation linked to modes of southern hemisphere climate variability, *J. Clim.*, *20*, 5418–5440.

Wallace, J. M., I. M. Held, D. W. J. Thompson, K. E. Trenberth, and J. E. Walsh (2014), Global warming and winter weather, *Science*, *343*.

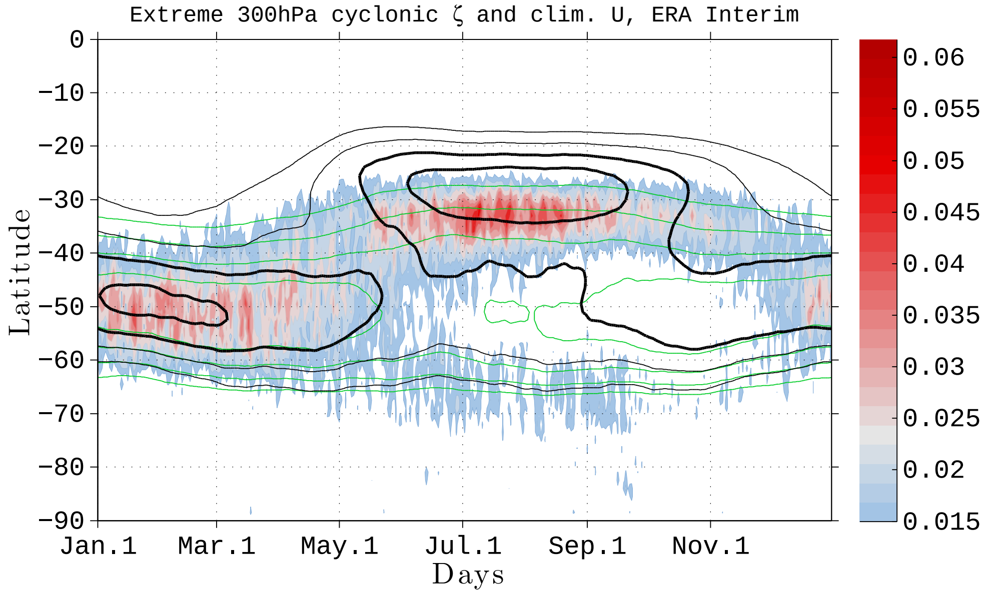

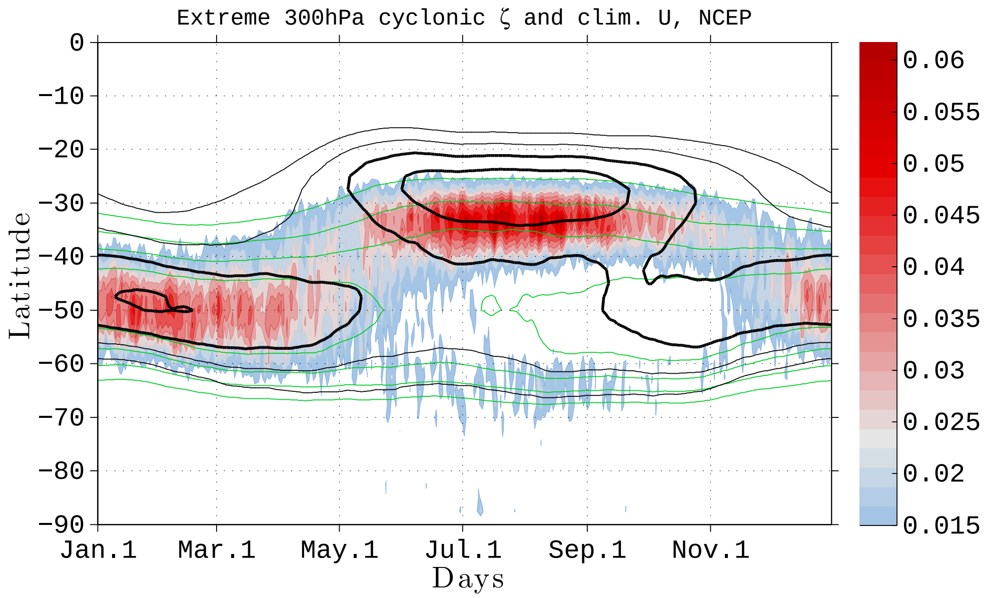

Figure 1. A daily-latitude plot of the fraction of the days (frequency of occurrence) with extremely low (below the 1^{st} percentile) 300 hPa vorticity values on a given calendar day and latitude, counting over all years and longitudes (colors), using two reanalyses data sets: a) ERA Interim. b) NCEP. Also shown in contours are the climatological zonal mean zonal winds at 300 hPa (black) and the $925-750$ hPa mean (green). The seasonal cycle is calculated by averaging each calendar day over all years, smoothed with a 21 day running mean.

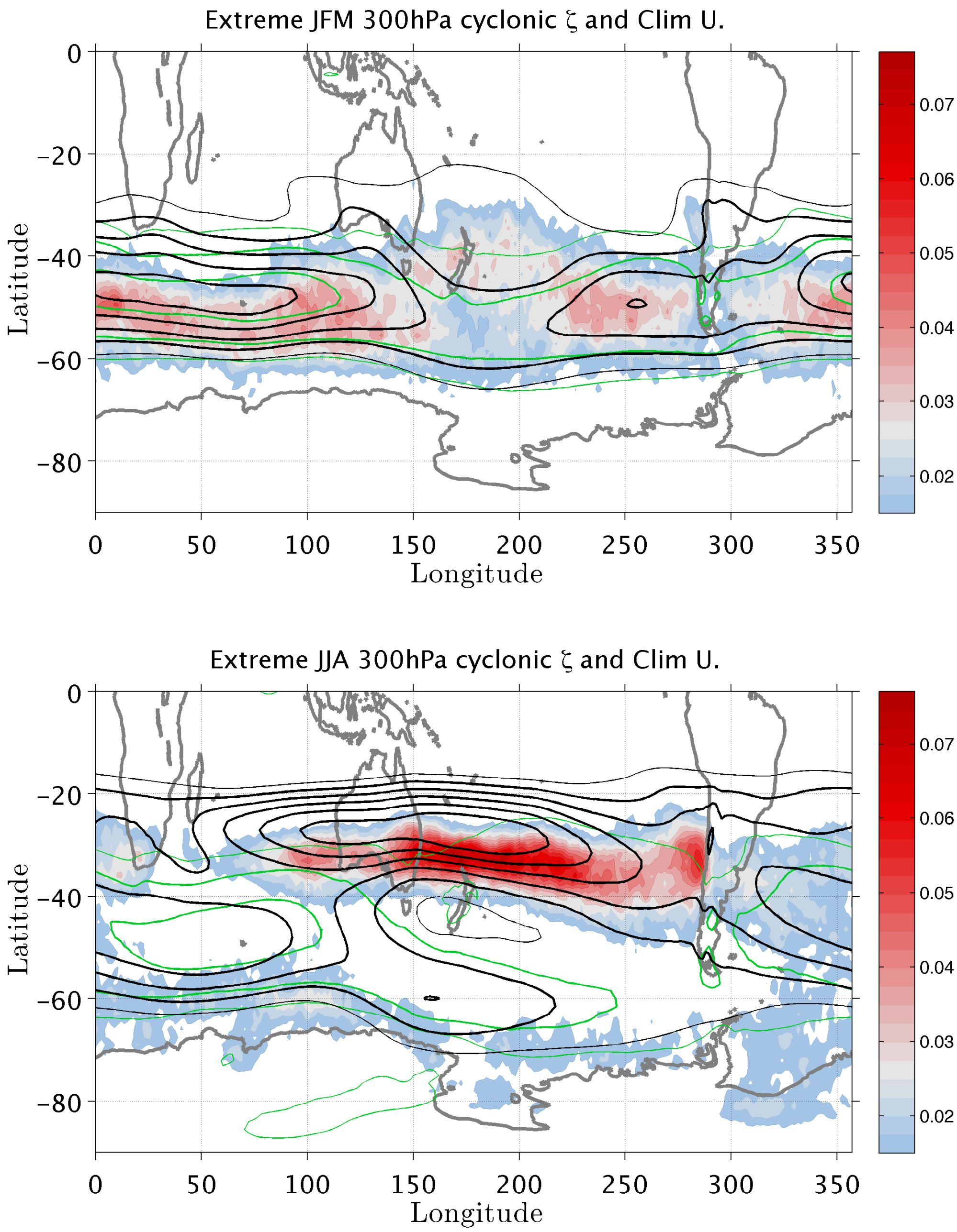

Figure 2. The seasonal mean distribution of the fraction of the days with extreme 300 hPa vorticity values at a given grid point (colors) from ERA Interim, counting over all seasons between 1979-2012 for the periods a) Jan-Mar, b) Jun-Aug. Also shown in contours on both graphs are the corresponding climatological seasonal mean zonal winds at 300 hPa (black) and the 925−750 hPa mean (green).

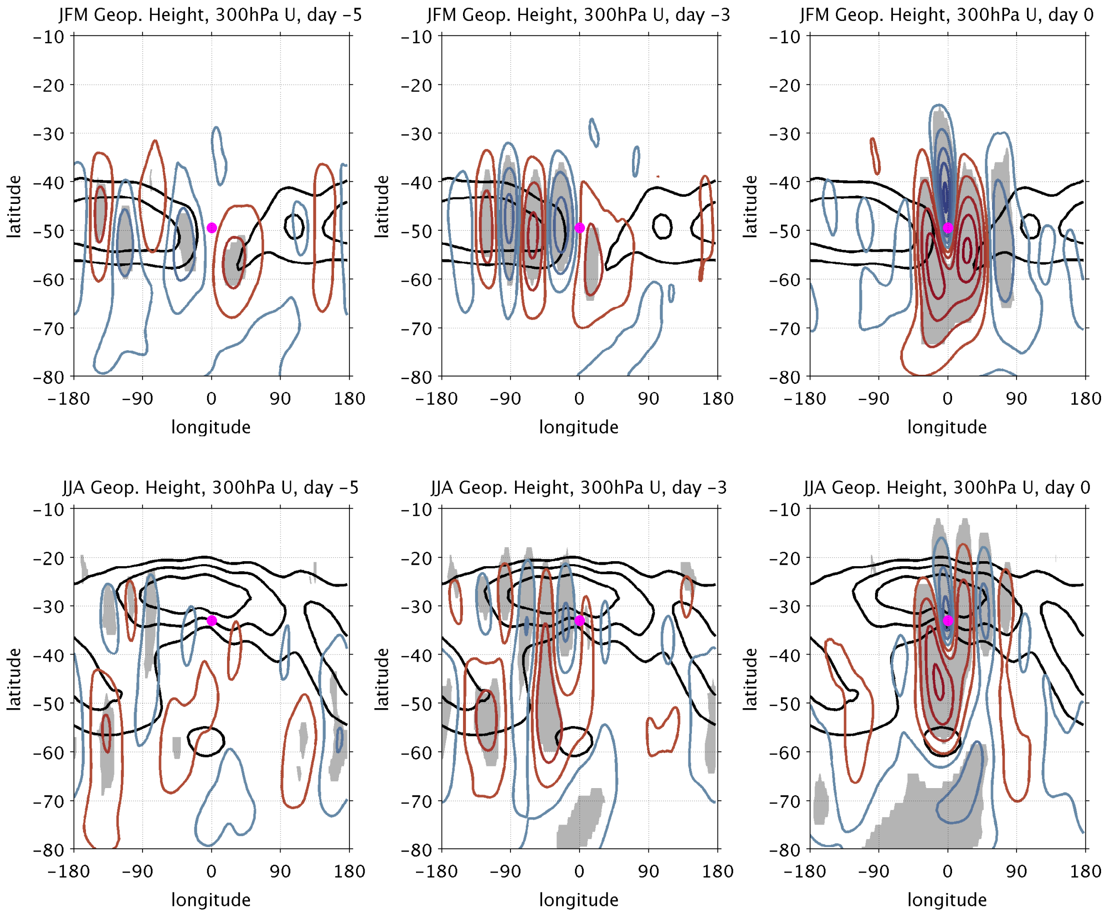

Figure 3. The longitudinally-centered composites of 300 hPa geopotential height anomalies for the most extreme negative vorticity events occurring at latitude 49.5^oS during Jan-Mar (top row) and at latitude 33^oS during Jun-Aug. Shown are the composites for days -5, -3, and 0 (left, middle and right, respectively), plotted on top of the zonal wind composite. For Jan-Mar (top row) the zonal winds are the respective day's composites while for Jun-Aug (bottom row) the mean of the composited fields for days $-6:6$ are shown. The shading marks the significant regions for geopotential height anomalies. Significance levels (99.9%) are determined based on a bootstrap method with respect to fields corresponding to characteristic vorticity wave packets. The Jan-Mar and Jun-Aug composites are based on the strongest 229 and 238 events respectively. Contour intervals for geopotential heights $\pm(15, 50:50:150)$, and for winds are $25, 30, 35$ m/sec

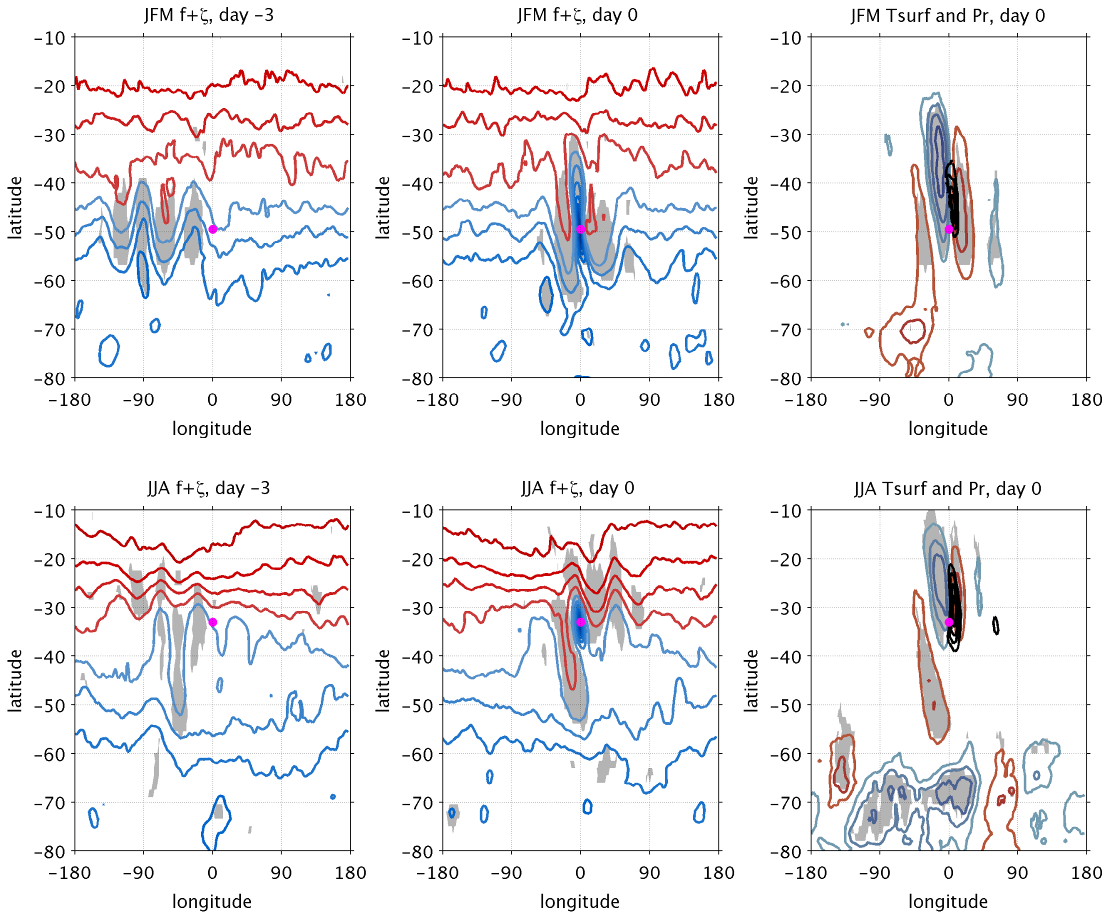

Figure 4. The longitudinally-centered composites of different fields, for the Jan-Mar and Jun-Aug extreme vorticity composites of Fig. 3 (top and bottom rows respectively). Shown are absolute vorticity at days -3 and 0 (left and middle plots) and the surface temperature anomaly alongside the total precipitation at day 0 (right plots). The shading marks the significant regions for absolute vorticity and surface temperature, while for precipitation, only significant values are plotted. Contour intervals for absolute vorticity are $(-1.4 : 0.2 : -0.4) \times 10^{-4}\ sec^{-1}$, for surface temperature anomalies are 0.5^oC (with maximal anomalies reaching $\pm 2^oC$) and for precipitation are $(6 : 2 : 12)\ mm/day$.